Technical Paper

Int'l J. of Aeronautical & Space Sci. 12(2), 179–189 (2011)
DOI:10.5139/IJASS.2011.12.2.179

IJASS
International Journal of Aeronautical and Space Science

Robust Adaptive Output Feedback Control Design for a Multi-Input Multi-Output Aeroelastic System

Z. Wang* and A. Behal**

Department of Electrical Engineering and Computer Science, University of Central Florida, NanoScience Technology Center, University of Central Florida, Orlando, FL, 32816

P. Marzocca***

Mechanical and Aeronautical Engineering, Clarkson University, Potsdam, NY, 1369

Abstract

In this paper, robust adaptive control design problem is addressed for a class of parametrically uncertain aeroelastic systems. A full-state robust adaptive controller was designed to suppress aeroelastic vibrations of a nonlinear wing section. The design used leading and trailing edge control actuations. The full state feedback (FSFB) control yielded a global uniformly ultimately bounded result for two-axis vibration suppression. The pitching and plunging displacements were measurable; however, the pitching and plunging rates were not measurable. Thus, a high gain observer was used to modify the FSFB control design to become an output feedback (OFB) design while the stability analysis for the OFB control law was presented. Simulation results demonstrate the efficacy of the multi-input multi-output control toward suppressing aeroelastic vibrations and limit cycle oscillations occurring in pre- and post-flutter velocity regimes.

Key words: Aeroelastic systems, Multi-input multi-output control, Robust adaptive control, Output feedback control

Nomenclature

α, h	= Pitching (rad) and plunging (m) displacements
β, γ	= Trailing and leading edge control surface (TECS and LECS) deflection (rad)
m_w, m_T	= Mass of wing and pitch-plunge system (kg)
m	= Airfoil mass per unit span (kg/m)
I_α	= Inertia of wing section about elastic axis (kg·m^2)
k_h, k_α	= Structural spring stiffness polynomials in plunging (N/m) and pitching (N·m)
C_h, C_α	= Structural damping coefficients in plunging (kg/s) and pitching (kg·m2/s)
a, b, s	= Mid-chord to elastic axis dimensionless distance, semi-chord (m) and wing section span (m)
$C_{l\alpha}$, $C_{m\alpha}$	= Rate of change of lift, moment w.r.t. angle-of-attack (1/rad)
$C_{m\alpha-eff}$	= Rate of change of effective moment w.r.t. angle-of-attack (1/rad)
$C_{l\beta}$, $C_{m\beta}$	= Rate of change of lift, moment w.r.t. TECS deflections (1/rad)
$C_{m\beta-eff}$	= Rate of change of effective moment w.r.t. TECS deflections (1/rad)
$C_{l\gamma}$, $C_{m\gamma}$	= Rate of change of lift, moment w.r.t. LECS deflections (1/rad)
$C_{m\gamma-eff}$	= Rate of change of effective moment w.r.t. LECS deflections (1/rad)
x_α	= Dimensionless static unbalance about the elastic axis

Received 20 May, 2011, Revised 3 June, 2011, Accepted 7 June, 2011

* Graduate Student
** Assistant Professor, Corresponding author
E-mail: abehal@ucf.edu Tel: +407-882-2820 Fax: +407-882-2819
*** Associate Professor

r_α = Dimensionless radius of gyration
U_∞, ρ_∞ = Freestream velocity (m/s) and air density (kg/m^3)
L, M = Aerodynamic lift (N) and moment (N·m)
x, u = Vector of system output, control input
h, f, G_s = System matrices
S, D, U = Factors of Gs
e_1, e_2, r, z = Tracking error, filtered tracking error, and composite error
K, k_T, Γ = Control and adaptation gains
T = Auxiliary control matrix
Y = Regression matrix
θ_1, θ_2, θ = Unknown constant parameters
$\hat{\theta}$, $\tilde{\theta}$ = Parameter estimates and mismatch error
α_1, a_2, $\bar{\varepsilon}$ = Observer constants

1. Introduction

Reduced weight, increased structural flexibility and operating speed certainly increase the likelihood of flutter occurring within the aircraft operational envelope. The mission profiles of next generation of flying vehicles will require adaptable airframes to best meet varying flight conditions. However, geometry changes could possibly incur aeroelastic instabilities, such as flutter, at transition points during the mission. New requirements imposed on the design next generation vehicles have called for increasing structural flexibility, and high maneuverability while maintaining the ability to operate safely in severe environmental conditions. Consequently, developing and implementing active control technology has become very important. In the last two decades, the advances in active control technology have rendered the applications of active flutter suppression and active vibrations control systems feasible. Great research efforts are currently devoted to the aeroelastic active control and flutter suppression of flight vehicles. Librescu and Marzocca (2005) presented state-of-the-art advances in these areas. Recent contributions related to the active control of an aircraft wing are discussed in length in a publication by Mukhopadhyay (2000a, b, 2011).

Behal et al. (2006b), Guijjula et al. (2005), Plantantis and Srganac (2004) presented novel research that improved the performance of adaptive schemes through wing extensions containing two control surfaces. Platanitis and Strganac (2004) presented an adaptive scheme that utilized full-state feedback. However, the uncertainty in the coupling between the control inputs was not taken into account. Rather, an inversion of the nominal input gain matrix was utilized to decouple the control inputs. Gujjula et al. (2005) designed adaptive and radial basis functions neural network controllers in order to compensate for system nonlinearity. Furthermore, a projection operator was utilized to assure that the input gain matrix estimate remained invertible. To sidestep the need for projection, Behal et al. (2006b) utilized a symmetric-triangular decomposition of the input gain matrix in order to design singularity free controllers for the leading edge control surfaces (LECS) and trailing edge control surfaces (TECS). This control design required full-state feedback as well as a filtered tracking error. Reddy et al. (2007) design an output feedback (OFB) adaptive controller that used backstepping coupled with a symmetric-diagonal-upper triangular factorization. Wang et al. (2011) proposed a modular OFB controller to suppress aeroelastic vibrations on an unmodeled nonlinear wing section subject to a variety of external disturbances. Wang et al. (2010a) presented a detailed report of the adaptive and robust control of nonlinear aeroelastic models.

As previously discussed, Behal et al. (2006a) and Reddy et al. (2007) proposed adaptive control algorithms that utilized a backstepping approach that led to significant over-parameterization and a very complicated control design. The adaptive control design work proposed in Behal et al. (2006b) does not utilize backstepping but the control design is full-state feedback which requires a measurement not only of the output variables but also their time derivatives.

The work in this paper removes the restrictions exhibited in the works by Behal et al. (2006a, b), Reddy et al. (2007). Consequently, the tracking error may converge to the origin. The work presented here exploited the robust adaptive OFB control scheme presented by Wang et al. (2010b).

The input gain matrix was assumed to be real with nonzero leading principal minors. By employing the matrix decomposition approach introduced by Morse (1993), the input gain matrix can be decomposed into the product of a

DOI:10.5139/IJASS.2011.12.2.179

symmetric p.d. matrix, a known diagonal matrix with +1 or -1 on the diagonal, and a unity upper triangular matrix. This triangular structure was exploited in the following adaptive control design and stability analysis since it allowed us to design algebraic loop-free control signals $u_i(t) \forall i = 1, 2$ sequentially. Next, the design of a full state feedback (FSFB) adaptive control law that yielded a global uniformly ultimately bounded (GUUB) result for the tracking error through a Lyapunov analysis was conducted. Finally, motivated by the high gain observer (HGO) presented by Atassi and Khalil (1999), an OFB control law was designed when only the system output vector was available for measurement. The simulation results on the 2-degree of freedom (DOF) wing section model show practical convergence under both FSFB and OFB control laws.

This paper is organized as follows. Section 2 introduces the system dynamics. Then, the control objective is defined and the open-loop error system is developed to facilitate the subsequent control design. Section 3 presents the robust adaptive feedback control design followed by a Lyapunov based analysis of stability of the closed-loop system. In Section 4, a solution based on a HGO is proposed to design the OFB controller. Simulation results to confirm the performance and robustness of the controller are presented in Section 5. Concluding remarks are provided in Section 6.

2. Aeroelastic Model Configuration and Error System Development

A 2-DOF pitch-plunge wing section based on previous models with both LECS and TECS is presented in Fig. 1. The system dynamics is given as follows

$$\begin{bmatrix} m_T & m_w x_\alpha b \\ m_w x_\alpha b & I_\alpha \end{bmatrix}\begin{bmatrix} \ddot{h} \\ \ddot{\alpha} \end{bmatrix}+\begin{bmatrix} c_h & 0 \\ 0 & c_\alpha \end{bmatrix}\begin{bmatrix} \dot{h} \\ \dot{\alpha} \end{bmatrix}+\begin{bmatrix} k_h & 0 \\ 0 & k_\alpha(\alpha) \end{bmatrix}\begin{bmatrix} h \\ \alpha \end{bmatrix}=\begin{bmatrix} -L \\ M \end{bmatrix}. \quad (1)$$

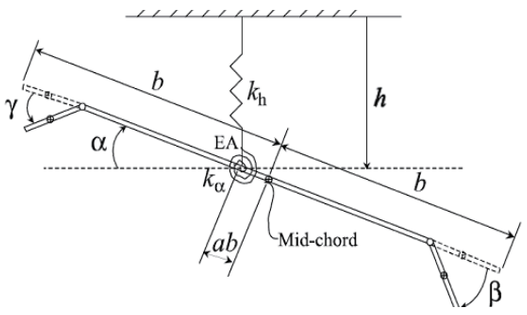

Fig. 1. Two degree of freedom aeroelastic system with both leading- and trailing-edge control surfaces.

In Eq. (1), the quasi-steady lift $L(\dot{h}, \dot{\alpha}, \alpha, \beta, \gamma)$ and aerodynamic moment $M(\dot{h}, \dot{\alpha}, \alpha, \beta, \gamma)$ are defined as

$$L = \rho U_\infty^2 bsC_{l\alpha}(\alpha + \tfrac{\dot{h}}{U_\infty} + (\tfrac{1}{2} - a)b\tfrac{\dot{\alpha}}{U_\infty}) + \rho U_\infty^2 bsC_{l\beta}\beta + \rho U_\infty^2 bsC_{l\gamma}\gamma, \quad (2)$$

$$M = \rho U_\infty^2 b^2 sC_{m\alpha-eff}(\alpha + \tfrac{\dot{h}}{U_\infty} + (\tfrac{1}{2} - a)b\tfrac{\dot{\alpha}}{U_\infty}) + \rho U_\infty^2 b^2 sC_{m\beta-eff}\beta + \rho U_\infty^2 b^2 sC_{m\gamma-eff}\gamma, \quad (3)$$

where $C_{m\alpha-eff}$, $C_{m\beta-eff}$, and $C_{m\gamma-eff}$ are given in the following form

$$\begin{aligned} C_{m\alpha-eff} &= (\tfrac{1}{2} + a)C_{l\alpha} + 2C_{m\alpha}, \\ C_{m\beta-eff} &= (\tfrac{1}{2} + a)C_{l\beta} + 2C_{m\beta}, \\ C_{m\gamma-eff} &= (\tfrac{1}{2} + a)C_{l\gamma} + 2C_{m\gamma}. \end{aligned} \quad (4)$$

The governing equation can be written into the input-output representation using Eqs. (2) and (3). Motivated by Chen et al. (2008) and Zhang et al. (2005), this representation will facilitate the ensuing robust adaptive feedback control design

$$\ddot{\mathbf{x}} = \mathbf{h}\left(\mathbf{x}, \dot{\mathbf{x}}, \boldsymbol{\theta}_1\right) + \mathbf{G}_s\mathbf{u}, \quad (5)$$

where $\mathbf{x} = [\alpha, h]^T \in R^2$ is a vector of system output and $\mathbf{u} = [u_1, u_2]^T = [\beta, \gamma]^T \in R^2$ denotes the control input vector. The drifting vector $\mathbf{h}(\mathbf{x}, \dot{\mathbf{x}}, \boldsymbol{\theta}_1)$, which is assumed to satisfy Lipschitz condition, contains uncertain nonlinearities due to the existence of $k_\alpha(\alpha)$. The input gain matrix G_{-s} can be explicitly given as follows

$$\mathbf{G}_s = \begin{bmatrix} g_{11} & g_{12} \\ g_{21} & g_{22} \end{bmatrix} \in \Re^{2\times 2}, \quad (6)$$

where the constant matrix entries g_{-ij} are defined as follows

$$\begin{aligned} g_{11} &= -U_\infty^2 \Delta^{-1}\rho bs\left(I_\alpha C_{l\beta} + m_w x_\alpha b^2 C_{m\beta-eff}\right), \\ g_{12} &= -U_\infty^2 \Delta^{-1}\rho bs\left(I_\alpha C_{l\gamma} + m_w x_\alpha b^2 C_{m\gamma-eff}\right), \\ g_{21} &= U_\infty^2 \Delta^{-1}\rho bs\left(m_w x_\alpha b C_{l\beta} + m_T b C_{m\beta-eff}\right), \\ g_{22} &= U_\infty^2 \Delta^{-1}\rho bs\left(m_w x_\alpha b C_{l\gamma} + m_T b C_{m\gamma-eff}\right), \end{aligned} \quad (7)$$

where $\Delta = \det(\mathbf{G}_s) = m_T I_\alpha - m_w^2 x_\alpha^2 b^2 \neq 0$. Based on the matrix decomposition introduced by Morse (1993) and the assumptions that both the leading principal minors g11 and Δ are non-zero, the input gain matrix $\mathbf{G}_{-s}$ can be decomposed as $\mathbf{G}_s = \mathbf{SDU}$ where **S** is a symmetric, positive-definite matrix, **D** is a diagonal matrix with diagonal entries +1 or -1, and **U** is an unknown unity upper triangular matrix. According to the **SDU** decomposition result previously obtained by Reddy et al. (2007), the explicit representation for **S**, **D**, and U can be given as

$$\mathbf{S}=\begin{bmatrix} |g_{11}| & \text{sign}(g_{11})g_{21} \\ \text{sign}(g_{11})g_{21} & \text{sign}(g_{11})\text{sign}(\Delta)[g_{22}-g_{11}^{-1}g_{21}(g_{12}-g_{21}\text{sign}(\Delta))] \end{bmatrix},$$

$$\mathbf{D}=\begin{bmatrix} \text{sign}(g_{11}) & 0 \\ 0 & \text{sign}(g_{11})\text{sign}(\Delta) \end{bmatrix}, \mathbf{U}=\begin{bmatrix} 1 & \frac{|g_{11}^{-1}|(g_{12}-g_{21}\text{sign}(\Delta))}{\text{sign}(g_{11})} \\ 0 & 1 \end{bmatrix}, \quad (8)$$

where the notation sign(*) represents the standard signum function. In this paper, the signs of the leading principal minors of the input gain matrix $\mathbf{G}_{-s}$ are assumed to be known for purposes of control design, which implies that the diagonal matrix **D** is known. After applying the matrix decomposition property and multiplying both sides of Eq. (5) with $\mathbf{M} = \mathbf{S}^{-1} \in R^{2\times2}$, Eq. (5) can be rewritten as

$$\mathbf{M}\ddot{\mathbf{x}} = \mathbf{f}\left(\mathbf{x}, \dot{\mathbf{x}}, \theta_2\right) + \mathbf{DUu}, \quad (9)$$

where M is a symmetric, positive definite matrix and $\mathbf{f}(\mathbf{x}, \dot{\mathbf{x}}, \boldsymbol{\theta}_1) = \mathbf{M}\cdot\mathbf{h}(\mathbf{x}, \dot{\mathbf{x}}, \boldsymbol{\theta}_2) \in R^2$ contains parametric nonlinearities. Note that M is assumed to be bounded by

$$\underline{m}\|\xi\|^2 \le \xi^T\mathbf{M}\xi \le \overline{m}\|\xi\|^2 \quad \forall \xi \in \Re^2, \quad (10)$$

where $\underline{m}$, $\overline{m} \in$ R are the minimum and maximum eigenvalues of the matrix **M**. The tracking error $\mathbf{e}_1(t) \in R^2$ for the aeroelastic system can be defined as $\mathbf{e}_1 = \mathbf{X}_d - \mathbf{X}$, where the desired output vector $\mathbf{x}_d(t) \in R^2$ can be zero all the time in this problem. Next, to simplify the subsequent control design, the auxiliary error signals $\mathbf{e}_2(t) \in R^2$ and filtered tracking error $\mathbf{r}(t) \in R^2$ are introduced as follows

$$\mathbf{e}_2 = \dot{\mathbf{e}}_1 + \mathbf{e}_1, \quad (11)$$

$$\mathbf{r} = \mathbf{e}_2 + \mathbf{e}_1. \quad (12)$$

Then, based on the above error system definitions, a composite error signal **z**(t) can be defined as follows

$$\mathbf{z} = \left[\mathbf{e}_1^T,\ \mathbf{r}^T\right]^T. \quad (13)$$

After taking the time derivative of r and substituting the derivative of e2, the following equation can be obtained as follows

$$\dot{\mathbf{r}} = \ddot{\mathbf{e}}_2 + 2\dot{\mathbf{e}}_1. \quad (14)$$

After multiplying both sides of Eq. (14) by M and applying the definitions given in Eqs. (9) and (12), Eq. (14) can be rewritten as

$$\mathbf{M}\dot{\mathbf{r}} = \mathbf{M}\left(\ddot{\mathbf{x}}_d + 2\dot{\mathbf{e}}_1\right) - \mathbf{f}\left(\mathbf{x}, \dot{\mathbf{x}}, \theta_2\right) - \mathbf{DUu}. \quad (15)$$

Furthermore, given a strictly upper triangular matrix $\overline{\mathbf{U}} = \mathbf{DU} - \mathbf{D}$, the open-loop dynamics of Eq. (15) can be rewritten as follows

$$\mathbf{M}\dot{\mathbf{r}} = \mathbf{M}\left(\ddot{\mathbf{x}}_d + 2\dot{\mathbf{e}}_1\right) - \mathbf{f}\left(\mathbf{x}, \dot{\mathbf{x}}, \theta_2\right) - \overline{\mathbf{U}}\mathbf{u} - \mathbf{Du}, \quad (16)$$

while above equation can be further rewritten as

$$\mathbf{M}\dot{\mathbf{r}} = \mathbf{Y}\left(\ddot{\mathbf{x}}_d, \dot{\mathbf{x}}, \mathbf{x}, \dot{\mathbf{e}}_1, \mathbf{e}_1, \mathbf{u}\right)\boldsymbol{\theta} - \mathbf{Du} - \mathbf{e}_1, \quad (17)$$

where the linear parameterization term $\mathbf{Y}(\ddot{\mathbf{x}}_d, \dot{\mathbf{x}}, \mathbf{x}, \dot{\mathbf{e}}_1, \mathbf{e}_1, \mathbf{u})$ $\theta \in R^2$ is defined as follows

$$\mathbf{Y}\left(\ddot{\mathbf{x}}_d, \dot{\mathbf{x}}, \mathbf{x}, \dot{\mathbf{e}}_1, \mathbf{e}_1, \mathbf{u}\right)\boldsymbol{\theta} = \mathbf{M}\left(\ddot{\mathbf{x}}_d + 2\dot{\mathbf{e}}_1\right) - \mathbf{f}\left(\mathbf{x}, \dot{\mathbf{x}}, \theta_2\right) - \overline{\mathbf{U}}\mathbf{u} + \mathbf{e}_1. \quad (18)$$

3. State Feedback Control Development

3.1 FSFB control design

In this section, all state variables in Eq. (1) are assumed to be available for measurement. To facilitate the ensuing control design, the following auxiliary control matrix is given as

$$\mathbf{T} = diag\left[\|Y_1\|^2 \quad \|Y_2\|^2\right] \in \Re^{2\times2}, \quad (19)$$

where Y_i denotes the ith row of the measurable regression matrix $\mathbf{Y} \in R^{2\times p}$. Based on previous definition as well as the subsequent stability analysis, the following state feedback adaptive control law is proposed

$$\mathbf{u}(t) = \mathbf{D}^{-1}\left(\mathbf{Y}\hat{\boldsymbol{\theta}} + \mathbf{Kr} + \mathbf{k}_T\mathbf{Tr}\right), \quad (20)$$

where K, $\mathbf{k}_T \in R^{2\times2}$ are positive-definite, diagonal gain matrices while $u_i \in R\ \forall\ i = 1, 2$ is the ith element of the control input vector u. Note that the robustifying term kTTr in Eq. (20) is used to ensure uniformity of the stability. The parameter adaptation law for $\boldsymbol{\theta}(t) \in R^p$ is given as follows

$$\dot{\hat{\boldsymbol{\theta}}} = Proj\left\{\boldsymbol{\Gamma}\mathbf{Y}^T\mathbf{r}, \hat{\boldsymbol{\theta}}\right\}, \quad (21)$$

where the constant adaptation gain matrix $\Gamma \in R^{p\times p}$ is diagonal and positive definite while p denotes the dimensions of the unknown parameter vector. Based on the results presented by Pomet and Praly (1992), the parameter projection operator *Proj*{·} is designed to bound parameter estimates $\hat{\boldsymbol{\theta}}(t)$ in a known compact set Ω_ε such that

$$\hat{\boldsymbol{\theta}}(t) \in \Omega_\varepsilon \quad \forall t > 0 \quad \text{if } \hat{\boldsymbol{\theta}}(0) \in \Omega_\varepsilon. \quad (22)$$

Note that the strict triangular structure of $\overline{\mathbf{U}}$ in Eq. (18) implies that u1 only depends on u2 but u2 can be determined independently of other control inputs since the diagonal elements in $\overline{\mathbf{U}}$ are all zero. Thus, the control law can be

implemented by designing u_{-2} first, then using that design in the computation of u_{-1}. After substituting Eq. (20) into the open-loop dynamics given in Eq. (17), and then multiplying both sides by **M**, the following closed-loop system dynamics can be obtained

$$\mathbf{M}\dot{\mathbf{r}} = -\mathbf{e}_1 - \mathbf{K}\mathbf{r} + \mathbf{Y}\tilde{\boldsymbol{\theta}} - \mathbf{k}_T\mathbf{T}\mathbf{r}, \tag{23}$$

where $\tilde{\boldsymbol{\theta}}(t) \in R^p$ is a parameter estimation error defined as follows

$$\tilde{\boldsymbol{\theta}}(t) = \boldsymbol{\theta} - \hat{\boldsymbol{\theta}}. \tag{24}$$

3.2 Stability analysis

In this section, a non-negative Lyapunov candidate function $V(t, \mathbf{z}) \in R$ is defined to analyze the stability of the full state feedback control law

$$V(t,\mathbf{z}) = \frac{1}{2}\mathbf{e}_1^T\mathbf{e}_1 + \frac{1}{2}\mathbf{r}^T\mathbf{M}\mathbf{r}, \tag{25}$$

which can be upper and lower bounded as

$$\alpha_1(\|\mathbf{z}\|) \le V \le \alpha_2(\|\mathbf{z}\|), \tag{26}$$

where $\alpha_1(\|\mathbf{z}\|)$ and $\alpha_2(\|\mathbf{z}\|)$ are class K_∞[4] functions given as

$$\alpha_1(\|\mathbf{z}\|) = \frac{1}{2}\min(1,\underline{m})\|\mathbf{z}\|^2, \quad \alpha_2(\|\mathbf{z}\|) = \frac{1}{2}\max(1,\bar{m})\|\mathbf{z}\|^2, \tag{27}$$

where the assumption stated in Eq. (10) has been utilized. After taking the time derivative of Eq. (25), and then substituting Eqs. (12) and (23), the following result for $V(t, \mathbf{z})$ can be obtained

$$\begin{aligned}\dot{V} &= \tfrac{1}{2}\mathbf{e}_1^T\dot{\mathbf{e}}_1 + \mathbf{r}^T\mathbf{M}\dot{\mathbf{r}} \\ &= -2\mathbf{e}_1^T\mathbf{e}_1 - \mathbf{r}^T\mathbf{K}\mathbf{r} + \mathbf{r}^T\mathbf{Y}\tilde{\boldsymbol{\theta}} - \mathbf{r}^T\mathbf{k}_T\mathbf{T}\mathbf{r}.\end{aligned} \tag{28}$$

By applying the expressions given in Eq. (19), the expression in Eq. (28) can be rewritten as follows

$$\dot{V} \le -2\mathbf{e}_1^T\mathbf{e}_1 - \mathbf{r}^T\mathbf{K}\mathbf{r} + \sum_{i=1}^{2}\left(\|\tilde{\theta}\|\|Y_i\|\|r_i\| - k_{T,i}\|Y_i\|^2\|r_i\|^2\right), \tag{29}$$

where k_T, i represents the ith diagonal element for the gain matrix kT. By adding and subtracting $\|\tilde{\theta}\|^2/4k_{T,1}$ and $\|\tilde{\theta}\|^2/4k_{T,2}$ to the right hand side of Eq. (29), the following result can be obtained

$$\begin{aligned}\dot{V} \le\ & -2\mathbf{e}_1^T\mathbf{e}_1 - \mathbf{r}^T\mathbf{K}\mathbf{r} - \left(\sqrt{k_{T,1}}\|Y_1\|\|r_1\| - \frac{\|\tilde{\theta}\|}{2\sqrt{k_{T,1}}}\right)^2 \\ & - \left(\sqrt{k_{T,2}}\|Y_2\|\|r_2\| - \frac{\|\tilde{\theta}\|}{2\sqrt{k_{T,2}}}\right)^2 + \frac{\|\tilde{\theta}\|^2}{4k_{T,1}} + \frac{\|\tilde{\theta}\|^2}{4k_{T,2}}.\end{aligned} \tag{30}$$

Then, $\dot{V}(t, \mathbf{z})$ can be further upperbounded as

$$\dot{V} \le -2\mathbf{e}_1^T\mathbf{e}_1 - \mathbf{r}^T\mathbf{K}\mathbf{r} + \left(\frac{\|\tilde{\theta}\|^2}{4k_{T,1}} + \frac{\|\tilde{\theta}\|^2}{4k_{T,2}}\right). \tag{31}$$

According to the definition of z(t) given in Eq. (13), the upperbound for $\dot{V}(t, \mathbf{z})$ in Eq. (31) can be expressed as

$$\dot{V} \le -\lambda_3\|\mathbf{z}\|^2 + \delta, \tag{32}$$

where $\lambda_3 = \min\{2, \lambda_{\min}(\mathbf{K})\}$ while $\lambda_{\min}(\mathbf{K})$ represents the minimum eigenvalue of **K**. The constant δ is given by

$$\delta = \frac{1}{2k}\sup_{\hat{\theta}\in\Omega_c}\|\tilde{\theta}\|^2, \quad k = \min(k_{T,1}, k_{T,2}), \tag{33}$$

where the supremum exists since parameter projection operator defined in Eq. (21) ensures the boundedness of the parameter estimates, which implies that the parameter estimates error is also bounded. From Eq. (32), it is also easy to show that

$$\dot{V} \le -\gamma(\|\mathbf{z}\|), \quad \forall\|\mathbf{z}\| > \varsigma > 0, \tag{34}$$

where $\varsigma = \sqrt{\lambda_3^{-1}\delta}$ while $\gamma(\|\mathbf{z}\|)$ is a positive-definite function. From the results in Eqs. (27) and (34), all conditions for the following theorem (Khalil, 1996) are satisfied.

Theorem 4.18 (Khalil, 1996): Let $D \subset R^n$ be a domain that contains the origin and $V:[0, \infty)\times D \to R$ be a continuously differentiable function such that

$$\begin{aligned}&\alpha_1(\|x\|) \le V(t,x) \le \alpha_2(\|x\|) \\ &\frac{\partial V}{\partial t} + \frac{\partial V}{\partial x}f(t,x) \le -W_3(x), \forall\|x\| \ge \mu > 0\end{aligned}$$

$\forall t \ge 0$ and $\forall x \ge D$, where α_1 and α_2 are class K functions and W3(x) is a continuous positive definite function. Take $r>0$ such that $B_r \subset D$ and suppose that

$\mu < \alpha_2^{-1}(\alpha_1(r))$

Then, there exists a class of KL function and for every initial state $x(t_0)$, satisfying $\|x(t_0)\| < \alpha_2^{-1}(\alpha_1(r))$, there is $T>0$ (dependent on x(t0) and μ) such that the solution of (4.32) satisfies

$$\begin{aligned}&\|x(t)\| \le \beta(\|x(t_0)\|, t-t_0), \forall t_0 \le t \le t_0 + T \\ &\|x(t)\| \le \alpha_1^{-1}(\alpha_2(\mu)), \forall t \ge t_0 + T\end{aligned}$$

Moreover, if $D = R^n$ and α_1 belongs to class $K\infty$, then the above two functions hold for any initial state $x(t_0)$, with no restriction on the magnitude of μ.

Thus, the error signal $\|\mathbf{z}\|$ is GUUB

$$\begin{aligned} \|\mathbf{z}\| &< \beta\left(\|\mathbf{z}_0\|,\ t-t_0\right),\ \forall t_0 < t \le t_0+T \\ \|\mathbf{z}\| &\le \alpha_1^{-1}\left(\alpha_2\left(\varsigma\right)\right),\ \forall t \ge t_0+T \end{aligned}, \tag{35}$$

where $\beta(\cdot,\cdot)$ is a class KL function while T depends on $\|\mathbf{z}_0\|$ and ς. From Eq. (33), kt can be made large enough such that the upper bound for $\|\mathbf{z}\|$ can be made arbitrarily small.

4. OFB Control Development

4.1 High gain observer

In this section, it is assumed that the only measurements available are the pitching and plunging displacements, while the remaining states can be estimated by using of HGO. An estimated composite error signal $\hat{z}(t) = [\hat{\mathbf{e}}_1^T, \mathbf{r}]^T \in R^4$ for the auxiliary error signal $\mathbf{z}(t)$ can be obtained via the following HGO (Atassi and Khalil, 1999)

$$\dot{\hat{\mathbf{e}}}_1 = \hat{\mathbf{r}} - 2\hat{\mathbf{e}}_1 + \frac{\alpha_1}{\bar{\varepsilon}}\left(\mathbf{e}_1 - \hat{\mathbf{e}}_1\right) \text{ and } \dot{\hat{\mathbf{r}}} = \frac{\alpha_2}{\bar{\varepsilon}^2}\left(\mathbf{e}_1 - \hat{\mathbf{e}}_1\right), \tag{36}$$

where $\alpha_i \in R\ \forall\ i = 1, 2$ are gain constants and $\bar{\varepsilon}$ is a small positive constant. In order to facilitate the analysis in the singularly perturbed form, the scaled observer errors $\eta(t) = \{\eta_1^T\ \eta_2^T]^T \in R^4$ can be defined as follows

$$\boldsymbol{\eta}_1(t) = \frac{1}{\bar{\varepsilon}}(\mathbf{e}_1 - \hat{\mathbf{e}}_1) \text{ and } \boldsymbol{\eta}_2(t) = \mathbf{r} - \hat{\mathbf{r}}. \tag{37}$$

Based on Eq. (37) as well as the definitions for $\hat{z}(t)$ and $\mathbf{z}(t)$, it's easily see that

$$\hat{\mathbf{z}} = \mathbf{z} - \mathbf{D}_\varepsilon \boldsymbol{\eta}, \tag{38}$$

where $D_\varepsilon \in R^{4\times4}$ can be given as follows
$\mathbf{D}_\varepsilon = diag\{\bar{\varepsilon}\ \mathbf{I}_2\ \mathbf{I}_2\}$.
After differentiating Eq. (37) as well as taking advantage of the definition in Eq. (11), Eq. (12) and the design of Eq. (36), the following observer error dynamics can be obtained

$$\begin{aligned} \bar{\varepsilon}\dot{\boldsymbol{\eta}}_1 &= -\alpha_1\boldsymbol{\eta}_1 + \boldsymbol{\eta}_2 - 2\bar{\varepsilon}\boldsymbol{\eta}_1 \\ \bar{\varepsilon}\dot{\boldsymbol{\eta}}_2 &= -\alpha_2\boldsymbol{\eta}_1 + \bar{\varepsilon}\dot{\mathbf{r}} \end{aligned}, \tag{39}$$

where $i = 1, 2$. Thus, a more compact form of Eq. (39) is represented as follows

$$\bar{\varepsilon}\dot{\boldsymbol{\eta}}(t) = \mathbf{A}_0\boldsymbol{\eta}(t) + \bar{\varepsilon}\mathbf{g}, \tag{40}$$

where $\mathbf{g} \in R^4$ is defined as follows

$$\mathbf{g} = \begin{bmatrix} -2\boldsymbol{\eta}_1^T & \dot{\mathbf{r}}^T \end{bmatrix}^T, \tag{41}$$

while $\alpha_i \forall\ i = 1, 2$ in Eq. (40) are chosen in a way such that

$$\mathbf{A}_0 = \begin{bmatrix} -\alpha_1\mathbf{I}_2 & \mathbf{I}_2 \\ -\alpha_2\mathbf{I}_2 & 0_m \end{bmatrix}$$

is Hurwitz. The boundary-layer system $\frac{d\eta(\tau)}{d\tau} = \mathbf{A}_0\eta(\tau)$ induces a Lyapunov candidate function $W(\eta) = \boldsymbol{\eta}^T\mathbf{P}_0\boldsymbol{\eta}$ which has the following properties

$$\begin{cases} \lambda_{\min}(\mathbf{P}_0)\|\boldsymbol{\eta}\|^2 \le W(\boldsymbol{\eta}) \le \lambda_{\max}(\mathbf{P}_0)\|\boldsymbol{\eta}\|^2 \\ \dot{W} = \frac{\partial W}{\partial \boldsymbol{\eta}}\dot{\boldsymbol{\eta}} \le -\|\boldsymbol{\eta}\|^2 \\ \left\|\frac{\partial W}{\partial \boldsymbol{\eta}}\right\| \le 2\|\mathbf{P}_0\|\|\boldsymbol{\eta}\|,\ \ \|\mathbf{P}_0\| = \lambda_{\max}(\mathbf{P}_0) \end{cases}. \tag{42}$$

Note that in the above equation, λ_{max} $(\mathbf{P}_0)$ denotes the maximum eigenvalue of $\mathbf{P}_{-0}$, while $\mathbf{P}_0 \in R$ is a p.d. matrix that satisfies $\mathbf{P}_0\mathbf{A}_0 + \mathbf{A}_0\mathbf{P}_0 = -\mathbf{I}_4$. From Eq. (42), it is clear that $\boldsymbol{\eta}(t) = 0$ is a globally exponentially stable equilibrium of the boundary-layer system.

4.2 OFB control law

From the observer error dynamic in Eq. (39), the solution of $\boldsymbol{\eta}(t)$ contains terms like $\frac{1}{\bar{\varepsilon}}e$ for some $\omega > 0$, which may introduce the so-called peaking phenomenon and cause instability. To suppress the peaking phenomenon on the state estimates, the full-state control design in Eq. (20) is modified to an OFB saturated control as follows (Atassi and Khalil, 1999)

$$\mathbf{u}(t) = \mathbf{D}^{-1}\left(\hat{\mathbf{Y}}\hat{\boldsymbol{\theta}} + \mathbf{K}sat\{\hat{\mathbf{r}}\} + \mathbf{k}_T\hat{\mathbf{T}}sat\{\hat{\mathbf{r}}\}\right), \tag{43}$$

where sat{} is the standard saturation function used to limit the magnitude of the control signal to avoid the peak phenomenon. $\hat{\mathbf{Y}}$ and $\hat{\mathbf{T}}$are the regression and auxiliary matrix defined in Eqs. (18) and (19) with respect to sat $\{\hat{\mathbf{z}}\}$ instead of z(t). $\mathbf{K}$, $\mathbf{k}_T$ are defined in Eq. (20), $\hat{\boldsymbol{\theta}}(t)$ is obtained through the projection algorithm in Eq. (21) with respect to $\hat{\mathbf{Y}}$ and $\hat{\mathbf{r}}$

$$\dot{\hat{\boldsymbol{\theta}}} = Proj\left\{\Gamma\hat{\mathbf{Y}}^T\hat{\mathbf{r}}, \hat{\boldsymbol{\theta}}\right\}. \tag{44}$$

The saturation of input is applied outside a compact set $D_c = \{\mathbf{z}(t) \in R^4 | V(t) < c\}$ of the region of attraction domain D_z. After substituting Eq. (43) into Eq. (17), it's easy to see that

$$\begin{aligned} \dot{\mathbf{r}} &= \boldsymbol{\varphi}\left(\mathbf{z}, \mathbf{D}_\varepsilon\boldsymbol{\eta}, t\right) \\ &= \mathbf{M}^{-1}\left[\mathbf{Y}\boldsymbol{\theta} - \mathbf{e}_1 + \hat{\mathbf{Y}}\hat{\boldsymbol{\theta}} + \mathbf{K}\hat{\mathbf{r}} + \mathbf{k}_T\left\|\hat{\mathbf{Y}}\right\|^2\hat{\mathbf{r}}\right]. \end{aligned} \tag{45}$$

After combining Eqs. (17, 40, 41, 45), the following closed-loop error dynamics are obtained

$$\begin{cases} \dot{\mathbf{z}}(t) & = \mathbf{f}_r\left(\mathbf{z}(t), \mathbf{D}_\varepsilon \eta(t), t\right) \\ \bar{\varepsilon}\dot{\eta}(t) & = \mathbf{A}_0 \eta(t) + \bar{\varepsilon}\mathbf{g}\left(\mathbf{z}(t), \mathbf{D}_\varepsilon \eta(t)\right). \end{cases} \tag{46}$$

4.3 OFB stability results

The OFB stability proof in this paper can be split into three steps in order to reduce the overall complexity. First, the existence of a positively invariant set for the solutions of Eq. (46) will be verified. Then, the boundedness of solutions of Eq. (46) is regained in the second step provided the trajectory ($\mathbf{z}(t)$, $\boldsymbol{\eta}(t)$) starts inside a compact subset of $D_z \times R^4$. Finally, global ultimate boundedness for Eq. (46) is recovered.

In the ensuing stability analysis, Z is defined to be any compact set in the interior of D_z such that $Z \subset D_c \subset D_z$, H is defined to be any compact set in the interior of R^4. Let D_ε = $\{\eta(t)\ R^4 \quad W(\eta(t)) \le \rho\bar{\varepsilon}^2\}$ be a compact set while $W(t)$ was defined in Eq. (42), ρ is a positive constant that is yet to be selected while $\bar{\varepsilon}$ is the HGO constant. In the following stability analysis, ($\mathbf{z}$(t), $\boldsymbol{\eta}(t)$) is considered to start inside $Z \times H$.

Theorem 1: (Invariant Set Theorem) Given $\sum = D_c \times D_\varepsilon$, there exists an $\bar{\varepsilon}_1 > 0$ such that $\forall \bar{\varepsilon} \in (0, \bar{\varepsilon}_1]$, $\sum$ is a positively invariant set for the trajectory ($\mathbf{z}$(t), η(t)).

First of all, given the following composite Lyapunov function $V_c(\mathbf{z}, \eta)$

$$V_c = V\left(\mathbf{z}\right) + W(\boldsymbol{\eta}), \tag{47}$$

where $V(\mathbf{z})$ and $W(\boldsymbol{\eta})$ have been previously defined in Eqs. (25) and (42). Then, after taking the time derivative of Eq. (47) along the trajectory of Eq. (46), it's straightforward to see that

$$\dot{V}_c = \dot{V} + \dot{W}, \tag{48}$$

where $\dot{V}(t)$ and $\dot{W}(t)$ can be further written as follows

$$\dot{V} = \frac{\partial V(\mathbf{z})}{\partial \mathbf{z}} f_r(\mathbf{z}(t), \mathbf{D}_\varepsilon \eta(t), t), \tag{49}$$

$$\dot{W} = \frac{\partial W(\boldsymbol{\eta})}{\partial \boldsymbol{\eta}}\left(\mathbf{A}_0 \eta(t)/\bar{\varepsilon} + \mathbf{g}(\mathbf{z}(t), \mathbf{D}_\varepsilon \eta(t), t)\right). \tag{50}$$

In this theorem, our goal is to prove that $\dot{V}_c|_{\partial\sum} \le 0$ while the notation ∂∑ denotes the boundary of the compact set ∑. Inside the set $\sum = D_c \times D_\varepsilon$, saturation does not apply on the control law. Thus, the term $\dot{V}(t)$ in Eq. (49) can be obtained as follows

$$\dot{V}(t) = -2\mathbf{e}_1^T\mathbf{e}_1 - \mathbf{r}^T\mathbf{K}\mathbf{r} + \mathbf{r}^T\left[\mathbf{Y}\tilde{\theta} - \mathbf{k}_T\mathbf{T}\mathbf{r}\right] + \mathbf{r}^T\left[\tilde{\mathbf{Y}}\hat{\theta} + \mathbf{K}\eta_2 + \mathbf{k}_T\mathbf{T}\eta_2\right], \tag{51}$$

where Eqs. (45) and (46) were utilized in above equation. By using the results in Eqs. (28) and (32), Eq. (51) can be rewritten as follows

$$\dot{V}(t) \le -\lambda_3\|\mathbf{z}\|^2 + \delta + \mathbf{r}^T\left[\tilde{\mathbf{Y}}\hat{\theta} + \mathbf{K}\eta_2 + \mathbf{k}_T\mathbf{T}\eta_2\right], \tag{52}$$

where $\tilde{\mathbf{Y}}(t) = \mathbf{Y} - \hat{\mathbf{Y}}$. When the closed loop solution is inside the invariant set ∑, the locally Lipschitz condition can be used on $\mathbf{h}(\mathbf{x}, \dot{\mathbf{x}}, \boldsymbol{\theta}_1)$ as well as the results in Eqs. (18) and (43) to prove the following inequalities

$$\left\|\tilde{\mathbf{Y}}\hat{\theta}\right\| \le \kappa_5\|\boldsymbol{\eta}\|, \tag{53}$$

$$\left\|\mathbf{K}\eta_2 + \mathbf{k}_T\mathbf{T}\eta_2\right\| + \kappa_5\|\boldsymbol{\eta}\|\|\mathbf{r}\| \le \kappa_4\|\boldsymbol{\eta}\|, \tag{54}$$

where k_4, $k_5 \in R$ are positive constants. Based on Eqs. (53) and (54), Eq. (52) can be rewritten as follows

$$\dot{V}(t) \le -\lambda_3\|\mathbf{z}\|^2 + \delta + \kappa_4\|\boldsymbol{\eta}\|. \tag{55}$$

From Eq. (42), it is straightforward to see that $\|\eta(t)\| \le \bar{\varepsilon}\sqrt{\rho/\lambda_{\min}\{\mathbf{P}_0\}}$ $\forall \eta(t) \in D_\varepsilon$. Therefore, Eq. (55) can be rewritten as follows

$$\dot{V}(t) \le -\lambda_3\|\mathbf{z}\|^2 + \delta + \kappa_4\bar{\varepsilon}\sqrt{\rho/\lambda_{\min}\{\mathbf{P}_0\}}. \tag{56}$$

From Eq. (26), any $c > 2\lambda_2\delta/\lambda_3$ and $\mathbf{z}(t) \in \partial D_c$ can follow $\frac{1}{2}\lambda_3\|\mathbf{z}\|^2 > \delta$. Based on above facts and Eq. (56), the following expression can be obtained

$$\dot{V}(t)|_{\partial D_c} \le -\frac{\lambda_3}{2}\|\mathbf{z}\|^2 + \kappa_4\bar{\varepsilon}\sqrt{\rho/\lambda_{\min}\{\mathbf{P}_0\}}. \tag{57}$$

Motivated by Eq. (57), ε_1 can be defined as $\varepsilon_1 = \frac{\beta}{k_4\sqrt{\lambda_{\min}\{\mathbf{P}_0\}/\rho}}$, where $\beta \in R$ is defined as follows

$$\beta = \min_{\mathbf{z}\in\partial D_c}\frac{\lambda_3}{2}\|\mathbf{z}\|^2. \tag{58}$$

Then $\forall 0 < \bar{\varepsilon} < \varepsilon_1$ and $\boldsymbol{\eta}(t) \in D_\varepsilon$, based on the result in Eq. (51), it is easy to see that

$$\dot{V}(t)|_{\partial D_c} \le 0. \tag{59}$$

Next, $\dot{W}(\cdot)$ of Eq. (50) can be upperbounded as follows

$$\dot{W} \le -\frac{1}{\bar{\varepsilon}}\|\boldsymbol{\eta}\|^2 + 2\|\mathbf{P}_0\|\|\boldsymbol{\eta}\|\|\mathbf{g}\|, \tag{60}$$

where $\mathbf{P}_0\mathbf{A}_0 + \mathbf{A}_0^T\mathbf{P}_0 = -\mathbf{I}_4$. By using Eq. (41) and the fact that $\bar{\varepsilon}$ is strictly less than 1, the following inequality can be obtained

$$\|\mathbf{g}\| \le 3\|\boldsymbol{\eta}\| + \|\dot{\mathbf{r}}\|. \tag{61}$$

Note that $\mathbf{z}(t)$ is bounded inside D_c which proves that $\|\mathbf{g}\| \le k_1\|\eta\| + k_2 \ \forall \ \mathbf{z}(t) \in D_c$ and $\boldsymbol{\eta}(t) \in R$ where k_1, $k_2 > 0$ are constants independent of $\bar{\varepsilon}$. This result further implies that

$$\begin{aligned}\dot{W}(t) \le \ & -\tfrac{1}{3\bar{\varepsilon}}\|\boldsymbol{\eta}\|^2 - \|\boldsymbol{\eta}\|^2\left(\tfrac{1}{3\bar{\varepsilon}} - 2\kappa_1\|\mathbf{P}_0\|\right) \\ & -\|\boldsymbol{\eta}\|\left(\tfrac{1}{3\bar{\varepsilon}}\|\boldsymbol{\eta}\| - 2\kappa_2\|\mathbf{P}_0\|\right).\end{aligned} \tag{62}$$

According to Eq. (42), $\|\eta\| \le \bar{\varepsilon}\sqrt{\rho/\|\mathbf{P}_0\|}$ given $\boldsymbol{\eta}(t) \in \partial D_\varepsilon$. Then, given a choice of $\varepsilon_2 < \dfrac{1}{6\|\mathbf{P}_0\|k_1}$, a choice of $\rho = 36k_2^2\|\mathbf{P}_0\|^3$ ensures the following result

$$\dot{W}(t)\,|_{\partial \mathfrak{b}_\varepsilon} \le -\frac{1}{3\bar{\varepsilon}}\|\boldsymbol{\eta}\|^2 \le 0. \tag{63}$$

$\forall\, 0 < \bar{\varepsilon} < \varepsilon_2$. Finally, by defining $\bar{\varepsilon}_1 = \min\{1, \varepsilon_2, \varepsilon_3\}$, Eq. (63) implies that $\sum = D_c \times D_\varepsilon$ is an invariant set $\forall\, \bar{\varepsilon} \in (0, \bar{\varepsilon}_1]$.

Theorem 2: (Boundedness Theorem) There exists an $\bar{\varepsilon}_2 \le \bar{\varepsilon}_1$ such that $\forall\, \bar{\varepsilon} \in (0, \bar{\varepsilon}_2]$, any trajectory $(\mathbf{z}(t), \boldsymbol{\eta}(t))$ that starts inside $Z \times H$ is bounded for all time.

By using the boundedness of $\mathbf{z}(0)$ and $\hat{\mathbf{z}}(0)$, the definition of Eq. (37) implies that $\|\boldsymbol{\eta}(0)\| \le \dfrac{k_6}{\bar{\varepsilon}}$ where $k_6 > 0$ is a positive constant. From the boundedness assertion on $\boldsymbol{\varphi}(\mathbf{z}(t), \boldsymbol{\eta}(t))$, in Eq. (45) in the set $D_c \times R^4$, and the closed-loop system dynamics in Eq. (46), it is also straightforward to see that $\mathbf{z}(t)$ meets the following linear time growth upperbound

$\|\mathbf{z}(t) - \mathbf{z}(0)\| \le k_3 t$,

where $k_3 > 0$ is a positive constant. Thus, the existence of a time T_c is shown to be independent of $\bar{\varepsilon}$ such that $\mathbf{z}(t) \in D_c$ $\forall\ t \in [0, T_c]$. Our aim in this theorem is to show that $\bar{\varepsilon}$ can be picked in such a way that if $\eta_i(t)$ starts outside the invariant set $\sum$, it can be made to enter the invariant set before $\mathbf{z}(t)$ can exit D_c. Proving this previous assertion would imply that the solution $(\mathbf{z}(t), \boldsymbol{\eta}(t))$ is in the invariant set $\sum$ at some time T_ε which indicates that it will stay there $\forall t \in [T_\varepsilon, \infty)$. Outside the invariant set, $W(\eta) \ge \bar{\varepsilon}^2 = 36k_2^2\|\mathbf{P}_0\|^3\,\bar{\varepsilon}^2$ which implies $\|\eta\| \ge \bar{\varepsilon}k_2\|\mathbf{P}_0\|$. Based on Eq. (63), $\dot{W}(\eta)$ can be upperbounded as

$$\dot{W} \le -\frac{1}{3\bar{\varepsilon}\|\mathbf{P}_0\|}W(\boldsymbol{\eta}). \tag{64}$$

By solving the above differential inequality, an upperbound for $W(\boldsymbol{\eta}(t))$ can be obtained as follows

$$W(\boldsymbol{\eta}(t)) \le W(0)\exp(-\sigma_1 t/\bar{\varepsilon}), \tag{65}$$

where $\sigma_1 = \dfrac{1}{3\|\mathbf{P}_0\|}$. Based on Eq. (42) and $\|\boldsymbol{\eta}(0)\| \le \dfrac{k_6}{\bar{\varepsilon}}$, Eq. (65) can be rewritten as follows

$$W(\boldsymbol{\eta}(t)) \le \frac{\sigma_2}{\bar{\varepsilon}^2}\exp(-\sigma_1 t/\bar{\varepsilon}), \tag{66}$$

where $\sigma_2 = k_6^2\|\mathbf{P}_0\|$. Based on Eq. (66), $0 < \bar{\varepsilon}_1 < \bar{\varepsilon}_2$ can become small enough so that $W(\eta(t))$ enters D_ε at a time $T_\varepsilon = \dfrac{\bar{\varepsilon}}{\sigma_1}\ln\left(\dfrac{\sigma_2}{\rho\bar{\varepsilon}^{2n}}\right) \le T_c/2 \ \forall\ \bar{\varepsilon} \in (0, \bar{\varepsilon}_2]$. Since $\eta(t)$ enters the invariant set D_ε in less than half the time it takes for $\mathbf{z}(t)$ to exit D_ε, $(\mathbf{z}(t), \boldsymbol{\eta}(t))$ enters $\sum$ during $[0, T_\varepsilon]$. Hence, $\mathbf{z}(t), \boldsymbol{\eta}(t) \in L\infty$ for all times $t \le T_\varepsilon$. For $t \in [0, T_\varepsilon]$, the trajectory $(\mathbf{z}(t), \eta(t))$ is bounded by virtue of Eq. (64) and Eq. (66). Thus, all closed-loop trajectories $(\mathbf{z}(t), \eta(t))$ starting in $Z \times H$ are bounded for all time.

Theorem 3: (Ultimately Boundedness Theorem) Given any solution $(\mathbf{z}(t), \boldsymbol{\eta}(t))$ that starts in $Z \times H$ and given any small $\bar{\delta} > \sqrt{8\lambda_3^{-1}\bar{\delta}}$, there exists an $0 < \bar{\varepsilon}_3(\bar{\delta}) < \bar{\varepsilon}_2$ and $T(\bar{\delta}) > 0$ such that $\|\mathbf{z}(t)\| \le \bar{\delta}/2$ and $\|\eta(t)\| \le \bar{\delta}/2 \,\forall\, t \ge T(\bar{\delta})$ and $\forall \bar{\varepsilon} \in (0, \bar{\varepsilon}_3]$.

Based on Eq. (66), $\lim_{\varepsilon \to 0} W(\eta(t)) = 0 \,\forall 0 < \bar{\varepsilon} < \bar{\varepsilon}_2$. Thus, for any given small value $\bar{\delta}$, it's clearly to see that $\varepsilon_3 = \varepsilon_3(\bar{\delta}) \le \bar{\varepsilon}_2$ such that $\forall \bar{\varepsilon} \in (0, \bar{\varepsilon}_3]$, the following upperbound can be defined

$$\|\eta(t)\| \le \bar{\delta}/2 \quad \forall\ t \ge T_{\varepsilon 3}(\bar{\delta}). \tag{67}$$

Inside the invariant set $\sum$, Eq. (56) can be utilized to obtain the following conclusion

$$\dot{V}(t) \le -\frac{\lambda_3}{2}\|\mathbf{z}\|^2 - \left(\frac{\lambda_3}{2}\|\mathbf{z}\|^2 - \mu\right), \tag{68}$$

where $\mu \in R$ is defined as follows

$$\mu = \delta + \kappa_4\bar{\varepsilon}\sqrt{\rho/\lambda_{\min}\{\mathbf{P}_0\}}. \tag{69}$$

Given a compact set $D_\mu = \{\mathbf{z}: \dfrac{\lambda_3}{2}\|\mathbf{z}\|^2 \le \mu\}$, then $\|\mathbf{z}(t)\| \notin D_\mu$ implies that $\dot{V}(t)$ can be upperbounded as follows

$$\dot{V}(t) \le -\frac{\lambda_3}{2}\|\mathbf{z}\|^2 \le 0, \tag{70}$$

which implies that V is decreasing outside D_μ. Define $D_v = \{V(\mathbf{z}) \le c_0(\bar{\varepsilon}) = \max_{z \in D_v} V(\mathbf{z})\}$; clearly, $D_\mu \subset D_v$ since $c_0(\bar{\varepsilon})$ is defined to be a non-decreasing scalar function. By choosing $\varepsilon_4 = \varepsilon_4(\bar{\delta}) \le \bar{\varepsilon}_2$ small enough such that the set D_μ is compact for all $\bar{\varepsilon} \le \varepsilon_4$, the set D_v is in the interior of D_c and $D_v \subset \{\mathbf{z}: \|\mathbf{z}(t)\| \le \bar{\delta}/2\}$. From above results and the upperbound in Eq. (70), it is straightforward to show that the set $\sum_{ub} = D_v \times D_\varepsilon$ is positively invariant. Moreover, any trajectory in $\sum$ will enter $\sum_{ub}$ in a finite time $T_{\varepsilon 4} = T_{\varepsilon 4}(\bar{\delta}) \,\forall\, \varepsilon \in (0, \varepsilon_4]$. Choosing $\bar{\varepsilon}_3 = \bar{\varepsilon}_3(\bar{\delta}) = \min\{\varepsilon_3, \varepsilon_4\}$ and $T(\bar{\delta}) = \max\{T_{\varepsilon 3}, T_{\varepsilon 4}\}$, then

$$\|\mathbf{z}(t)\| + \|\boldsymbol{\eta}(t)\| \le \bar{\delta} \qquad \forall t \ge T(\bar{\delta}) \tag{71}$$

Thus $(\mathbf{z}(t), \boldsymbol{\eta}(t))$ starting in $Z \times H$ are ultimately bounded.

5. Simulations and Results

5.1 Model and control parameters

The simulation results are presented in the following paragraphs for a nonlinear 2-DOF aeroelastic system controlled by TECS and LECS. The nonlinear wing section model was simulated using the dynamics of Eqs. (1-3). The model parameters utilized in the simulation were the same as used by Platanitis and Strganac (2004) and are listed in Table 1.

The desired trajectory variables $\mathbf{x}_d$ $\mathbf{x}_d$ and $\dot{\mathbf{x}}_d$ were simply selected as zero. The initial conditions for pitch angle $\alpha(t)$ and plunge displacement $h(t)$ were selected as $\alpha(0) = 5.729$ deg and $h(0) = 0$ m while all other variables $\dot{h}(t)$, $\dot{\alpha}(t)$, $\ddot{h}(t)$, $\ddot{\alpha}(t)$, and the parameter estimates were also set to zero. In the simulation, the signs of the leading principal minors of the input gain matrix Gs were embedded in the diagonal matrix D which can be given as

$$\mathbf{D} = \begin{bmatrix} -1 & 0 \\ 0 & -1 \end{bmatrix}. \tag{72}$$

The magnitude of both the leading edge $\beta(t)$ and trailing edge $r(t)$ flaps was limited to 15 deg. Since the control design contained an adaptation scheme that involved integration of the filtered error signal r in Eq. (21), the control input saturation led to the windup problem. The following approach to limit the error signal $\hat{\mathbf{r}}$ was proposed according to the magnitude of original control input u_i (Astrom and Rundqwist, 1986)

$$r_{b,i} = \begin{cases} \hat{r}_i \dfrac{u_b}{|u_i|} & , \ |u_i| > u_b, \ \forall i = 1,2 \\ \hat{r}_i & , \ |u_i| \le u_b, \ \forall i = 1,2 \end{cases}, \tag{73}$$

Table 1. Wing section parameters

Parameter	Value	Parameter	Value
a	-0.4	b	0.135 m
I_α	0.065 kg · m^2	ρ_∞	1.225 kg/m3
m	12.387 kg	x_a	[0.07873 – (b + ab)]/b
c_h	27.43 kg/s	C_α	0.036 9 N · s
$C_{l\alpha}$	6.28 1/rad	$C_{m\alpha}$	(0.5 + a) 1/rad
$C_{l\beta}$	3.358 1/rad	$C_{m\beta}$	- 0.635 1/rad
k_h, i	2,844.4	k_α, i	2.8, 62.3, 3,709.7, 24,195.6, 48,756.9

where $\mathbf{r}_b$ denotes the limited filtered error and is used in the parameter update law Eq. (21) while u, designed in Eq. (43), denotes the actual control signal for the actuator with saturation bound u_b = 15 deg. The OFB control was implemented via the HGO defined in Eq. (36) and control law in Eq. (43). The parameters for the controller and observer in these simulations are listed in Table 2.

5.2 Results

The open-loop response of the system at pre-flutter speed $U_\infty = 8\text{m/s} < U_F = 11.4\text{ m/s}$ and post-flutter speed $U_\infty = 13.28\text{m/s} > U_F = 11.4$ m/s is given in Fig. 2. From Fig. 3, the convergence of the error to the origin under the proposed robust adaptive method is shown. During the pre-flutter speed, the proposed method exhibited faster settling times while the limit cycle oscillations (LCOs) at the post-flutter speed regimes were totally suppressed. In Fig. 3b, the system was allowed to evolve uncontrolled to produce LCOs due to the nonlinear pitch stiffness. The control was turned on at t = 5 s.

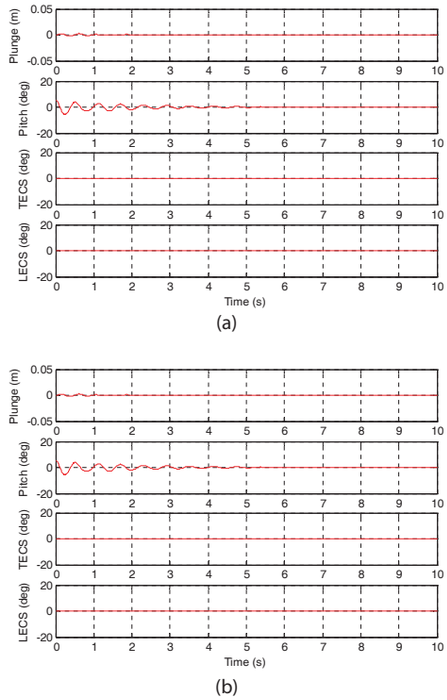

Fig. 2. Open-loop response (a) at pre-flutter speed U_∞ = 8 m/s; (b) at post-flutter speed U_∞ = 13.28 m/s. LECS: leading edge control surface, TECS: trailing edge control surface.

Table 2. Simulation parameters

Freestream velocity	K_{-11}	K_{-22}	K_{-T}	$Gamma_{-11}$	$Gamma_{-22}$	$alpha_{-1}$	$alpha_{-2}$	$\bar{\varepsilon}$
8 m/s	10	2	1	0.001	0.001	1	0.5	0.0005
13.28 m/s	4	2	0.01	5	5	1	0.5	0.0005

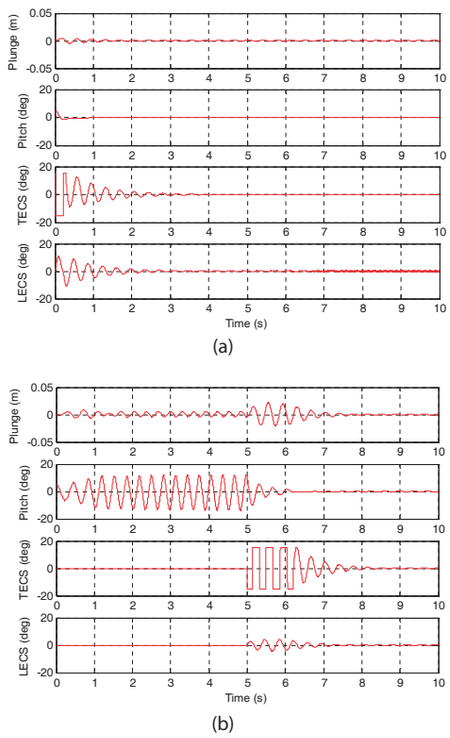

Fig. 3. Closed-loop response (a) at pre-flutter speed U_∞ = 8 m/s; (b) at post-flutter speed U_∞ = 13.28 m/s. LECS: leading edge control surface, TECS: trailing edge control surface.

6. Conclusions

A robust adaptive OFB controller was proposed to suppress parametrically uncertain aeroelastic vibrations on the wing section model. The control strategy was implemented via leading (γ) and trailing (β)-edge control surfaces. The system structure and parameters, with the exception of the signs of the principal minors of the input matrix, were assumed to be unknown in the control design. By using a Lyapunov based method for design and analysis, GUUB results were obtained on the two-axis vibration errors. HGO was used to design OFB control when only the output displacements were measurable. Future work will include the experimental evaluation of the robust adaptive controller in the wind-tunnel laboratory at Clarkson University.

References

Astrom, K. J. and Rundqwist, L. (1989). Integrator windup and how to avoid it. *Proceedings of American Control Conference*, Pittsburgh, PA. pp. 1693-1698.

Atassi, A. N. and Khalil, H. K. (1999). A separation principle for the stabilization of a class of nonlinear systems. *IEEE Transactions on Automatic Control*, 44, 1672-1687.

Behal, A., Marzocca, P., Rao, V. M., and Gnann, A. (2006a). Nonlinear adaptive control of an aeroelastic two-dimensional lifting surface. *Journal of Guidance, Control, and Dynamics*, 29, 382-390.

Behal, A., Rao, V. M., Marzocca, P., and Kamaludeen, M. (2006b). Adaptive control for a nonlinear wing section with multiple flaps. *Journal of Guidance, Control, and Dynamics*, 29, 744-749.

Chen, J., Behal, A., and Dawson, D. M. (2008). Robust feedback control for a class of uncertain MIMO nonlinear systems. *IEEE Transactions on Automatic Control*, 53, 591-596.

Gujjula, S., Singh, S. N., and Yim, W. (2005). Adaptive and neural control of a wing section using leading- and trailing-edge surfaces. *Aerospace Science and Technology*, 9, 161-171.

Khalil, H. K. (1996). *Nonlinear Systems*. 2nd ed. Upper Saddle River, NJ: Prentice Hall.

Librescu, L. and Marzocca, P. (2005). Advances in the linear/nonlinear control of aeroelastic structural systems. *Acta Mechanica*, 178, 147-186.

Morse, A. S. (1993). A gain matrix decomposition and some of its applications. *Systems and Control Letters*, 21, 1-10.

Mukhopadhyay, V. (2000a). Benchmark active control technology special section: part II. *Journal of Guidance Control and Dynamics*, 23, 1093-1093.

Mukhopadhyay, V. (2000b). Benchmark active control technology: part I. *Journal of Guidance Control and Dynamics*, 23, 913-913.

Mukhopadhyay, V. (2001). Benchmark active control technology special section: part III. *Journal of Guidance Control and Dynamics*, 24, 146-146.

Platanitis, G. and Strganac, T. W. (2004). Control of a nonlinear wing section using leading- and trailing-edge surfaces. *Journal of Guidance, Control, and Dynamics*, 27, 52-58.

Pomet, J. B. and Praly, L. (1992). Adaptive nonlinear regulation: estimation from the Lyapunov equation. *IEEE Transactions on Automatic Control*, 37, 729-740.

Reddy, K. K., Chen, J., Behal, A., and Marzocca, P. (2007). Multi-input/multi-output adaptive output feedback control design for aeroelastic vibration suppression. *Journal of Guidance, Control, and Dynamics*, 30, 1040-1048.

Wang, Z., Behal, A., and Marzocca, P. (2010a). Adaptive and robust aeroelastic control of nonlinear lifting surfaces with single/multiple control surfaces: a review. *International Journal of Aeronautical and Space Sicences*, 11, 285-302.

DOI:10.5139/IJASS.2011.12.2.179

Wang, Z., Behal, A., and Marzocca, P. (2011). Model-free control design for multi-input multi-output aeroelastic system subject to external disturbance. *Journal of Guidance, Control, and Dynamics*, 34, 446-458.

Wang, Z., Chen, J., and Behal, A. (2010b). Robust adaptive control design for a class of uncertain MIMO nonlinear systems. *IEEE International Symposium on Intelligent Control*, Yokohama, Japan. pp. 2284-2289.

Zhang, X., Behal, A., Dawson, D. M., and Xian, B. (2005). Output Feedback Control for a Class of Uncertain MIMO Nonlinear Systems With Non-Symmetric Input Gain Matrix, *IEEE Conference on Decision and Control*, Seville, Spain, pp. 7762-7767, December 2005.